

© 2007. The American Astronomical Society. All rights reserved. Access to this work was provided by the University of Maryland, Baltimore County (UMBC) ScholarWorks@UMBC digital repository on the Maryland Shared Open Access (MD-SOAR) platform.

Please provide feedback

Please support the ScholarWorks@UMBC repository by emailing scholarworks-group@umbc.edu and telling us

what having access to this work means to you and why it's important to you. Thank you.

The WEBT Campaign on the Blazar 3C 279 in 2006¹

M. Böttcher², S. Basu², M. Joshi², M. Villata³, A. Arai⁴, N. Aryan⁵, I. M. Asfandiyarov⁶, U. Bach³, R. Bachev⁷, A. Berduygin⁸, M. Blæk⁹, C. Buemi¹², A. J. Castro-Tirado¹¹, A. De Ugarte Postigo¹¹, A. Frasca¹², L. Fuhrmann^{30,13,3}, V. A. Hagen-Thorn¹⁷, G. Henson¹⁴, T. Hovatta¹⁶, R. Hudec⁹, M. Ibrahimov⁶, Y. Ishii⁴, R. Ivanidze¹⁵, M. Jelínek¹¹, M. Kamada⁴, B. Kapanadze¹⁵, M. Katsuura⁴, D. Kotaka⁴, Y. Y. Kovalev^{30,31}, Yu. A. Kovalev³¹, P. Kubánek⁹, M. Kurosaki⁴, O. Kurtanidze¹⁵, A. Lähteenmäki¹⁶, L. Lanteri³, V. M. Larionov¹⁷, L. Larionova¹⁷, C.-U. Lee¹⁸, P. Leto¹⁰, E. Lindfors⁸, E. Marilli¹², K. Marshall¹⁹, H. R. Miller¹⁹, M. G. Mingaliev³², N. Mirabal²⁰, S. Mizoguchi⁴, K. Nakamura⁴, E. Nieppola¹⁶, M. Nikolashvili¹⁵, K. Nilsson⁸, S. Nishiyama⁴, J. Ohlert²¹, M. A. Osterman¹⁹, S. Pak²³, M. Pasanen⁸, C. S. Peters²⁴, T. Pursimo²⁵, C. M. Raiteri³, J. Robertson²⁶, T. Robertson²⁷, W. T. Ryle¹⁹, K. Sadakane⁴, A. Sadun⁵, L. Sigua¹⁵, B.-W. Sohn¹⁸, A. Strigachev⁷, N. Sumitomo⁴, L. O. Takalo⁸, Y. Tamesue⁴, K. Tanaka⁴, J. R. Thorstensen²⁴, G. Tosti¹³, C. Trigilio¹², G. Umama¹², S. Vennes²⁶, S. Vitek¹¹, A. Volvach²⁸, J. Webb²⁹, M. Yamanaka⁴, H.-S. Yim¹⁷,

²Astrophysical Institute, Department of Physics and Astronomy,
Clippinger 339, Ohio University, Athens, OH 45701, USA

³Istituto Nazionale di Astrofisica (INAF), Osservatorio Astronomico di Torino,
Via Osservatorio 20, I-10025 Pino Torinese, Italy

⁴Astronomical Institute, Osaka Kyoiku University, Kashiwara-shi,
Osaka, 582-8582 Japan

⁵Department of Physics, University of Colorado at Denver,
Campus Box 157, P. O. Box 173364, Denver, CO 80217-3364, USA

⁶Ulugh Beg Astronomical Institute, Academy of Sciences of Uzbekistan,
33 Astronomical Str., Tashkent 700052, Uzbekistan

⁷Institute of Astronomy, Bulgarian Academy of Sciences,
72 Tsarigradsko Shosse Blvd., 1784 Sofia, Bulgaria

⁸Tuorla Observatory, University of Turku, 21500 Piikkiö, Finland

⁹Astronomical Institute, Academy of Sciences of the Czech Republic,
CZ-251 65 Ondrejov, Czech Republic

¹⁰Istituto di Radioastronomia, Sezione di Noto, C. da Renna Bassa –
Loc. Casa di Mezzo C. P. 141, I-96017 Noto, Italy

¹¹Instituto de Astrofisica de Andalucia, Apartado de Correos, 3004, E-18080 Granada, Spain

¹²Osservatorio Astrofisico di Catania, Viale A. Doria 6,
I-95125 Catania, Italy

¹³Osservatorio Astronomico, Università di Perugia, Via B. Bonfigli,
I-06126 Perugia, Italy

¹⁴East Tennessee State University and SARA Observatory,
Department of Physics, Astronomy, and Geology, Box 70652, Johnson City, TN 37614

¹⁵Abastumani Observatory, 383762 Abastumani, Georgia

¹⁶Metsähovi Radio Observatory, Helsinki University of Technology,
Metsähovintie 114, 02540 Kylmälä, Finland

¹⁷Astronomical Institute, St. Petersburg State University,
Universitetskyy pr. 28, Petrodvoretz, 198504 St. Petersburg, Russia

¹⁸Korea Astronomy & Space Science Institute, 61-1 Whaam-Dong, Yuseong-Gu,
Daejeon 305-348, Korea

¹⁹Department of Physics and Astronomy, Georgia State University,
Atlanta, GA 30303, USA

²⁰Department of Astronomy, University of Michigan,
830 Dennison Building, Ann Arbor, MI 48109-1090, USA

ABSTRACT

The quasar 3C 279 was the target of an extensive multiwavelength monitoring campaign from January through April 2006. An optical-IR-radio monitoring campaign by the Whole Earth Blazar Telescope (WEBT) collaboration was organized around Target of Opportunity X-ray and soft γ -ray observations with *Chandra* and *INTEGRAL* in mid-January 2006, with additional X-ray coverage by *RXTE* and *Swift* XRT. In this paper we focus on the results of the WEBT campaign.

The source exhibited substantial variability of optical flux and spectral shape, with a characteristic time scale of a few days. The variability patterns throughout the optical BVRI bands were very closely correlated with each other, while there was no obvious correlation between the optical and radio variability. After the ToO trigger, the optical flux underwent a remarkably clean quasi-exponential decay by about one magnitude, with a decay time scale of $\tau_d \sim 12.8$ d.

²¹Michael Adrian Observatory, Astronomie-Stiftung Trebur, Fichtenstrae 7, D-65468 Trebur, Germany

²³Department of Astronomy and Space Science, Kyung Hee University, Seocheon, Gilheung, Yongin, Gyeonggi, 446-701, South Korea

²⁴Department of Physics and Astronomy, Dartmouth College, MS 6127, Hannover, NH 03755, USA

²⁵Nordic Optical Telescope, Apartado 474, E-38700 Santa Cruz de La Palma, Santa Cruz de Tenerife, Spain

²⁶Florida Institute of Technology and SARA Observatory, 150 West University Boulevard, Melbourne, FL 32901-6975, USA

²⁷Ball State University and SARA Observatory, Department of Physics and Astronomy, Muncie, IN 47306, USA

²⁸Crimean Astrophysical Observatory, Nauchny, Crimea 98409, Ukraine

²⁹Florida International University and SARA Observatory, University Park Campus, Miami, FL 33199, USA

³⁰Max-Planck-Institut für Radioastronomie, Auf dem Hügel 69, D-53121 Bonn, Germany

³¹Astro Space Center of Lebedev Physical Institute, Profsoyuznaya 84/32, Moscow 117997, Russia

³²Special Astrophysical Observatory, Nizhnij Arkhyz, Karachai-Cherkessia 369167, Russia

In intriguing contrast to other (in particular, BL Lac type) blazars, we find a lag of shorter-wavelength behind longer-wavelength variability throughout the RVB wavelength ranges, with a time delay increasing with increasing frequency. Spectral hardening during flares appears delayed with respect to a rising optical flux. This, in combination with the very steep IR-optical continuum spectral index of $\alpha_o \sim 1.5 - 2.0$, may indicate a highly oblique magnetic field configuration near the base of the jet, leading to inefficient particle acceleration and a very steep electron injection spectrum.

An alternative explanation through a slow (time scale of several days) acceleration mechanism would require an unusually low magnetic field of $B \lesssim 0.2$ G, about an order of magnitude lower than inferred from previous analyses of simultaneous SEDs of 3C 279 and other FSRQs with similar properties.

Subject headings: galaxies: active — Quasars: individual (3C 279) — gamma-rays: theory — radiation mechanisms: non-thermal

1. Introduction

Flat-spectrum radio quasars (FSRQs) and BL Lac objects are active galactic nuclei (AGNs) commonly unified in the class of blazars. They exhibit some of the most violent high-energy phenomena observed in AGNs to date. Their spectral energy distributions (SEDs) are characterized by non-thermal continuum spectra with a broad low-frequency component in the radio – UV or X-ray frequency range and a high-frequency component from X-rays to γ -rays. Their electromagnetic radiation exhibits a high degree of linear polarization in the optical and radio bands and rapid variability at all wavelengths. Radio interferometric observations often reveal radio jets with individual components exhibiting apparent superluminal motion. At least episodically, a significant portion of the bolometric flux is emitted in > 100 MeV γ -rays. 46 blazars have been detected and identified with high confidence in high energy (> 100 MeV) γ -rays by the *Energetic Gamma-Ray Experiment Telescope (EGRET)* instrument on board the *Compton Gamma-Ray Observatory (CGRO)*, Hartman et al. 1999; Mattox, Hartman, & Reimer 2001).

In the framework of relativistic jet models, the low-frequency (radio – optical/UV) emission from blazars is interpreted as synchrotron emission from nonthermal electrons in a

¹For questions regarding the availability of the data from the WEBT campaign presented in this paper, please contact the WEBT President Massimo Villata at villata@oato.inaf.it

relativistic jet. The high-frequency (X-ray – γ -ray) emission could either be produced via Compton upscattering of low frequency radiation by the same electrons responsible for the synchrotron emission (leptonic jet models; for a recent review see, e.g., Böttcher 2007a), or due to hadronic processes initiated by relativistic protons co-accelerated with the electrons (hadronic models, for a recent discussion see, e.g., Mücke & Protheroe 2001; Mücke et al. 2003).

The quasar 3C279 ($z = 0.538$) is one of the best-observed flat spectrum radio quasars, not at last because of its prominent γ -ray flare shortly after the launch of *CGRO* in 1991. It has been persistently detected by *EGRET* each time it was observed, even in its very low quiescent states, e.g., in the winter of 1992 – 1993, and is known to vary in γ -ray flux by roughly two orders of magnitude (Maraschi et al. 1994; Wehrle et al. 1998). It has been monitored intensively at radio, optical, and more recently also X-ray frequencies, and has been the subject of intensive multiwavelength campaigns (e.g., Maraschi et al. 1994; Hartman et al. 1996; Wehrle et al. 1998).

Also at optical wavelengths, 3C 279 has exhibited substantial variability over up to two orders of magnitude ($R \sim 12.5 - 17.5$). Variability has been observed on a variety of different time scales, from years, down to intra-day time scales. The most extreme variability patterns include intraday variability with flux decays of $\lesssim 0.1^{\text{mag}}/\text{hr}$ (Kartalpepe & Balonek 2007). Observations with the *International Ultraviolet Explorer* in the very low activity state of the source in December 1992 – January 1993 revealed the existence of a thermal emission component, possibly related to an accretion disk, with a luminosity of $L_{\text{UV}} \sim 2 \times 10^{46} \text{ erg s}^{-1}$ if this component is assumed to be emitting isotropically (Pian et al. 1999). Pian et al. (1999) have also identified an X-ray spectral variability trend in archival *ROSAT* data, indicating a lag of $\sim 2 - 3$ days of the soft X-ray spectral hardening behind a flux increase. Weak evidence for spectral variability was also found within the *EGRET* (MeV – GeV) energy range (Nandikotkur et al. 2007). At low γ -ray flux levels, an increasing flux seems to be accompanied by a spectral softening, while at high flux levels, no consistent trend was apparent.

The quasar 3C 279 was the first object in which superluminal motion was discovered (Whitney et al. 1971; Cotton et al. 1979; Unwin et al. 1989). Characteristic apparent speeds of individual radio components range up to $\beta_{\text{app}} \sim 17$ (Cotton et al. 1979; Homan et al. 2003; Jorstad et al. 2004), indicating pattern flow speeds with bulk Lorentz factors of up to $\Gamma \sim 17$. Radio jet components have occasionally been observed not to follow straight, ballistic trajectories, but to undergo slight changes in direction between parsec- and kiloparsec-scales (Homan et al. 2003; Jorstad et al. 2004). VLBA polarimetry indicates that the electric field vector is generally well aligned with the jet direction on pc to kpc scales (Jorstad et al. 2004;

Ojha et al. 2004; Lister & Homan 2005; Helmboldt et al. 2007), indicating that the magnetic field might be predominantly perpendicular to the jet on those length scales.

A complete compilation and modeling of all available SEDs simultaneous with the 11 *EGRET* observing epochs has been presented in Hartman et al. (2001a). The modeling was done using the time-dependent leptonic (SSC + EIC) model of Böttcher, Mause, & Schlickeiser (1997); Böttcher & Bloom (2000) and yielded quite satisfactory fits for all epochs. The results were consistent with other model fitting works (e.g., Bednarek 1998; Sikora et al. 2001; Moderski et al. 2003) concluding that the X-ray – soft γ -ray portion of the SED might be dominated by SSC emission, while the *EGRET* emission might require an additional, most likely external-Compton, component. The resulting best-fit parameters were consistent with an increasing bulk Lorentz factor, but decreasing Lorentz factors of the ultrarelativistic electron distribution in the co-moving frame of the emission region during γ -ray high states, as compared to lower γ -ray states (Hartman et al. 2001a). However, such an interpretation also required changes of the overall density of electrons, and the spectral index of the injected electron power-law distribution, which did not show any consistent trend with γ -ray luminosity.

Hartman et al. (2001b) have investigated cross correlations between different wavelength ranges, in particular, between optical, X-ray, and γ -ray variability. In that work, a general picture of a positive correlation between optical, X-ray and γ -ray activity emerged, but no consistent trends of time lags between the different wavelength ranges were found.

The discussion above illustrates that, in spite of the intensive past observational efforts, the physics driving the broadband spectral variability properties of 3C 279 are still rather poorly understood. For this reason, Collmar et al. (2007b) proposed an intensive multiwavelength campaign in an optical high state of 3C 279, in order to investigate its correlated radio – IR – optical – X-ray – soft γ -ray variability. The campaign was triggered on Jan. 5, 2006, when the source exceeded an R-band flux corresponding to $R = 14.5$. It involved intensive radio, near-IR (JHK), and optical monitoring by the Whole Earth Blazar Telescope (WEBT², see, e.g. Raiteri et al. 2006; Villata et al. 2007, and references therein) collaboration through April of 2006, focusing on a core period of Jan. and Feb. 2006. In order to illustrate the source’s behaviour leading up to the trigger in January 2006, previously unpublished radio and optical data from late 2005 are also included in the analysis presented in this paper. X-ray and soft γ observations were carried out by all instruments on board the *International Gamma-Ray Astrophysics Laboratory (INTEGRAL)* during the period of Jan. 13 – 20, 2006. Additional, simultaneous X-ray coverage was obtained by *Chandra* and *Swift*

²<http://www.to.astro.it/blazars/webt>

XRT. These observations were supplemented by extended X-ray monitoring with the *Rossi X-Ray Timing Explorer (RXTE)*. In this paper, we present details of the data collection, analysis, and results of the WEBT (radio – IR – optical) campaign. Preliminary results of the multiwavelength campaign have been presented in Collmar et al. (2007a) and Böttcher (2007a,b), and a final, comprehensive report on the result of the entire multiwavelength campaign will appear in Collmar et al. (2007b).

Throughout this paper, we refer to α as the energy spectral index, F_ν [Jy] $\propto \nu^{-\alpha}$. A cosmology with $\Omega_m = 0.3$, $\Omega_\Lambda = 0.7$, and $H_0 = 70$ km s $^{-1}$ Mpc $^{-1}$ is used. In this cosmology, and using the redshift of $z = 0.538$, the luminosity distance of 3C 279 is $d_L = 3.1$ Gpc.

2. Observations, data reduction, and light curves

3C 279 was observed in a coordinated multiwavelength campaign at radio, near-IR, optical (by the WEBT collaboration), X-ray (*Chandra*, *Swift*, *RXTE PCA*, *INTEGRAL JEM-X*), and soft γ -ray (*INTEGRAL*) energies. The overall timeline of the campaign, along with the measured long-term light curves at radio and optical frequencies is illustrated in Fig. 1. Simultaneous X-ray coverage with all X-ray / soft γ -ray telescopes mentioned above was obtained in the time frame Jan. 13 – 20, as indicated by the gray shaded area in Fig. 1. Detailed results of those high-energy observations will be presented in Collmar et al. (2007b). Table 1 lists all participating observatories which contributed data to the WEBT campaign. In total, 25 ground-based radio, infrared, and optical telescopes in 12 countries on 4 continents contributed 2173 data points.

2.1. Optical and near-infrared observations

The observing strategy and data analysis followed to a large extent the standard procedure for the optical data reduction for WEBT campaigns which is briefly outlined below. For more information on standard data reduction procedures for WEBT campaigns see also: Villata et al. (2000); Raiteri et al. (2001); Villata et al. (2002); Böttcher et al. (2003); Villata et al. (2004a,b); Raiteri et al. (2005); Böttcher et al. (2005)

It had been suggested that, optimally, observers perform photometric observations alternately in the B and R bands, and include complete (U)BVRI sequences at the beginning and the end of each observing run. Exposure times should be chosen to obtain an optimal compromise between high precision (instrumental errors less than ~ 0.03 mag for small telescopes and ~ 0.01 mag for larger ones) and high time resolution. If this precision re-

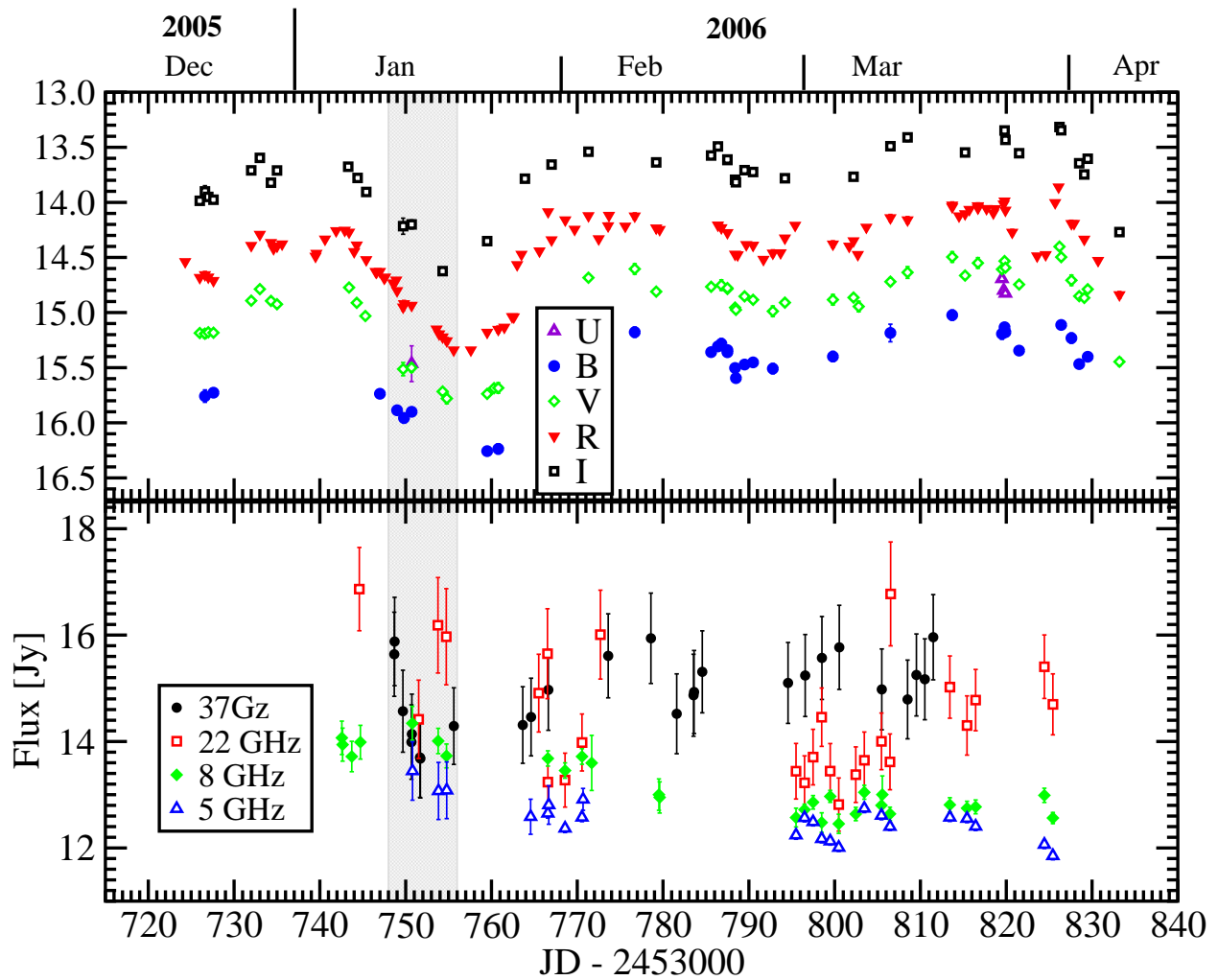


Fig. 1.— Timeline of the broadband campaign on 3C 279 in 2006, including the optical and radio light curves during the entire campaign period. The gray shaded area indicates the period of the *INTEGRAL*, *Chandra*, and *Swift* observations.

Table 1. List of observatories that contributed data to the WEBT campaign

| Observatory | Specifications | frequency / filters | N_{obs} |
|-------------------------------------|----------------|--------------------------|------------------|
| Radio | | | |
| Metsähovi, Finland | 14 m | 37 GHz | 70 |
| Medicina, Italy | 32 m | 5, 8, 22 GHz | 32 |
| Noto, Italy | 32 m | 8, 22 GHz | 6 |
| RATAN-600, Russia | 576 m (ring) | 1, 2.3, 5, 8, 11, 22 GHz | 138 |
| Crimean Astr. Obs., Ukraine (RT-22) | 22 m | 36 GHz | 7 |
| Infrared | | | |
| Roque (NOT), Canary Islands | 2.56 m | J, H, K | 3 |
| Optical | | | |
| Abastumani, Georgia (FSU) | 70 cm | R | 127 |
| ARIES, Naintal, India | | R | 63 |
| Belogradchik, Bulgaria | 60 cm | V, R, I | 75 |
| BOOTES-1, Spain | 30 cm | R | 151 |
| Catania, Italy | 91 cm | U, B, V | 33 |
| Crimean Astr. Obs., Ukraine | 70 cm | B, V, R, I | 47 |
| SMARTS, CTIO, Chile | 90 cm | B, V, R | 33 |
| Kitt Peak (MDM), Arizona, USA | 130 cm | U, B, V, R, I | 190 |
| Kitt Peak (MDM), Arizona, USA | 240 cm | R | 77 |
| Michael Adrian Obs., Germany | 120 cm | R | 9 |
| Mt. Lemmon, Arizona, USA | 100 cm | B, V, R, I | 214 |
| Mt. Maidanak (AZT-22), Uzbekistan | 150 cm | B, V, R, I | 44 |
| Osaka Kyoiku, Japan | 51 cm | V, R, I | 494 |
| Roque (KVA), Canary Islands | 35 cm | R | 75 |
| Roque (NOT), Canary Islands | 256 cm | U, B, V, R, I | 7 |
| SARA, Arizona, USA | 90 cm | B, V, R, I | 242 |
| Tenagra, Arizona, USA | 81 cm | B, V, R, I | 19 |
| Torino, Italy | 105 cm | B, V, R | 3 |
| Tuorla, Finland | 103 cm | R | 84 |

quirement leads to gaps of 15 – 20 minutes in each light curve, we suggested to carry out observations in the R band only. Observers were asked to perform bias and dark corrections as well as flat-fielding on their frames, and obtain instrumental magnitudes, applying either aperture photometry (using IRAF or CCDPHOT) or Gaussian fitting for the source 3C 279 and four recommended comparison stars. This calibration has then been used to convert instrumental to standard photometric magnitudes for each data set. In the next step, unreliable data points (with large error bars at times when higher-quality data points were available) were discarded. Our data did not provide evidence for significant variability on sub-hour time scales. Consequently, error bars on individual data sets could be further reduced by re-binning on time scales of typically 15 – 20 min. The data resulting at this stage of the analysis are displayed in the top panel of Fig. 1.

In order to provide information on the intrinsic broadband spectral shape (and, in particular, a reliable extraction of B - R color indices), the data were then de-reddened using the Galactic Extinction coefficients of Schlegel et al. (1998), based on $A_B = 0.123$ mag and $E(B - V) = 0.029$ mag³.

Possible contaminations of the optical color information could generally also arise from contributions from the host galaxy and the optical – UV emission from an accretion disk around the central supermassive black hole in 3C 279. However, these contributions are not expected to be significant in the case of our campaign data: Assuming absolute magnitudes of $M_V \sim -23$ and $M_B \sim -21$ for typical quasar host galaxies at $z \sim 0.5$ (e.g. Floyd et al. 2004; Zakamska et al. 2006), their contribution in the V and B band, respectively, at the distance of 3C 279 would be $V_{\text{gal}} \sim 19.5$ and $B_{\text{gal}} \sim 21.6$, respectively. These are at least about four magnitudes fainter than the actually measured total B and V magnitudes during our campaign, and thus negligible. The possible contribution of an accretion disk can be estimated on the basis of the thermal component for which Pian et al. (1999) found evidence in IUE observations during the 1992/1993 low state of 3C 279. Their best fit to this component suggests $U \sim 18.6$ and $B \sim 21$ (and much fainter contributions at lower frequencies), which corresponds to a contribution of $\lesssim 2.5$ % to the total B and U magnitudes measured during our campaign. Therefore, both the host galaxy and the accretion disk contribution are neglected in our further analysis.

The only infrared observations obtained for this campaign were one sequence of JHK exposures taken on January 15, 2006, with the 2.56 m NOT on Roque de los Muchachos on the Canary Island of La Palma. The resulting fluxes are included in the SED displayed in Fig. 8.

³<http://nedwww.ipac.caltech.edu/>

2.1.1. Optical light curves

The optical (and radio) light curves from December 2005 to April 2006 are displayed in Fig. 1. The densest coverage was obtained in the R band, and the figure clearly indicates that the variability in B, V, and I bands closely tracks the R-band behaviour. The coverage in the U band was extremely sparse and does not allow any assessment of the U-band light curve during our campaign. Therefore, the U-band will be ignored in the following discussion, and we will describe the main features of the variability behavior based on the R-band light curve.

The optical light curves show variability with magnitude changes of typically $\lesssim 0.5^{\text{mag}}$ on time scales of a few days. The most notable exception to this relatively moderate variability is the major dip of the brightnesses in all optical bands right around our coordinated X-ray / soft γ -ray observations in January 2006 (\approx JD 2453742 – 2453770). In the R-band, the light curve followed an unusually clean exponential decay over 1.1 mags. in 13 days, i.e., a slope of $dR/dt = 0.085$ mag/day or a flux decay as $F(t) = F(t_0) e^{-(t-t_0)/\tau_d}$ with a decay constant of $\tau_d = 12.8$ d. Only moderate intraday deviations on a characteristic scale of $\lesssim 0.1$ mag/d are superposed on this smooth exponential decay.

In contrast to the smooth decline of the optical brightness during January 6 – 20, 2006, the subsequent re-brightening to levels comparable to those before the dip, appears much more erratic and involves a remarkably fast rise by $\sim 0.5^{\text{mag}}$ within ~ 1 d on Jan. 27 (JD 2453763). Unfortunately, the detailed shape of this fast rise was not well sampled in our data set. If this was a quasi-exponential rise with a slope of $dR/dt \sim 0.5$ mag/d, it would correspond to a rise time scale of $\tau_r \sim 2.2$ d.

2.2. Radio observations

At radio frequencies, 3C 279 was monitored using the 14 m Metsähovi Radio Telescope of the Helsinki University of Technology, at 37 GHz, the 32-m radio telescope of the Medicina Radio Observatory near Bologna, Italy, at 5, 8, and 22 GHz, the 32-m antenna of the Noto Radio Observatory on Sicily, Italy, at 8 and 22 GHz, the 576-m ring telescope (RATAN-600) of the Russian Academy of Sciences, at 1, 2.3, 5, 8, 11, and 22 GHz, and the 22-m RT-22 dish at the Crimean Astrophysical Observatory, Ukraine, at 36 GHz.

The Metsähovi data have been reduced with the standard procedure described in Teräsranta et al. (1998). The resulting 37 GHz light curve is reasonably well sampled during the period mid-January – mid-March 2006. Inspection by eye in comparison to the optical light curves displayed in Fig. 1 appears to indicate that the optical and 37 GHz light curves follow simi-

lar variability patterns with a radio lead before the optical variability by ~ 5 days. However, a discrete cross-correlation analysis between the R-band and 37 GHz radio light curves did not reveal a significant signal to confirm this suggestion.

Also included in Fig. 1 are the radio light curves at 5, 8, and 22 GHz. For details of the analysis of data from the Medicina and Noto radio observatories at those frequencies, see Bach et al. (2007). As already apparent in Fig. 1, most of the data at frequencies below 37 GHz were not well sampled on the $\lesssim 3$ -months time scale of the 2006 campaign, and any evidence for variability did not show a discernable correlation with the variability at higher (radio and optical) frequencies.

All radio data contributed to this campaign are stored in the WEBT archive (see <http://www.to.astro.it/blazars/webt/> for information regarding availability of the data). Radio data at all observed frequencies have been included in the quasi-simultaneous SED for Jan 15, 2006, shown in Fig. 8. Given the generally very moderate radio variability at frequencies below 37 GHz, a linear interpolation between the two available data points nearest in time to Jan. 15, 2006, was used to construct an estimate of the actual radio fluxes at that time.

3. Optical spectral variability

In this section, we will describe spectral variability phenomena, i.e. the variability of spectral (and color) indices and their correlations with monochromatic source fluxes. We will concentrate here on the optical spectral variability as indicated by a change of the optical color. In particular, our observing strategy was optimized to obtain a good sampling of the B – R color index as a function of time. Since our data did generally not indicate substantial flux changes on sub-hour time scales, we extracted B – R color indices wherever both magnitudes were available within 20 minutes of each other. Fig. 2 shows the B – R color history over the entire campaign, compared to the B and R band light curves. Overall, there is no obvious correlation between the light curves and the color behavior of the source on long time scales. However, two short-term sequences attracted our attention: There is a sequence of brightness decline accompanied by a spectral hardening (declining B – R index) around JD 2453750 (Jan. 14, 2006), and another sequence of a brightness increase accompanied by a spectral softening around JD 2453790 – 2453806 (Feb. 23 – Mar. 11). However, we caution that incomplete sampling, in particular in the B-band may introduce spurious effects.

A similar trend was recently observed in a multiwavelength WEBT campaign on the

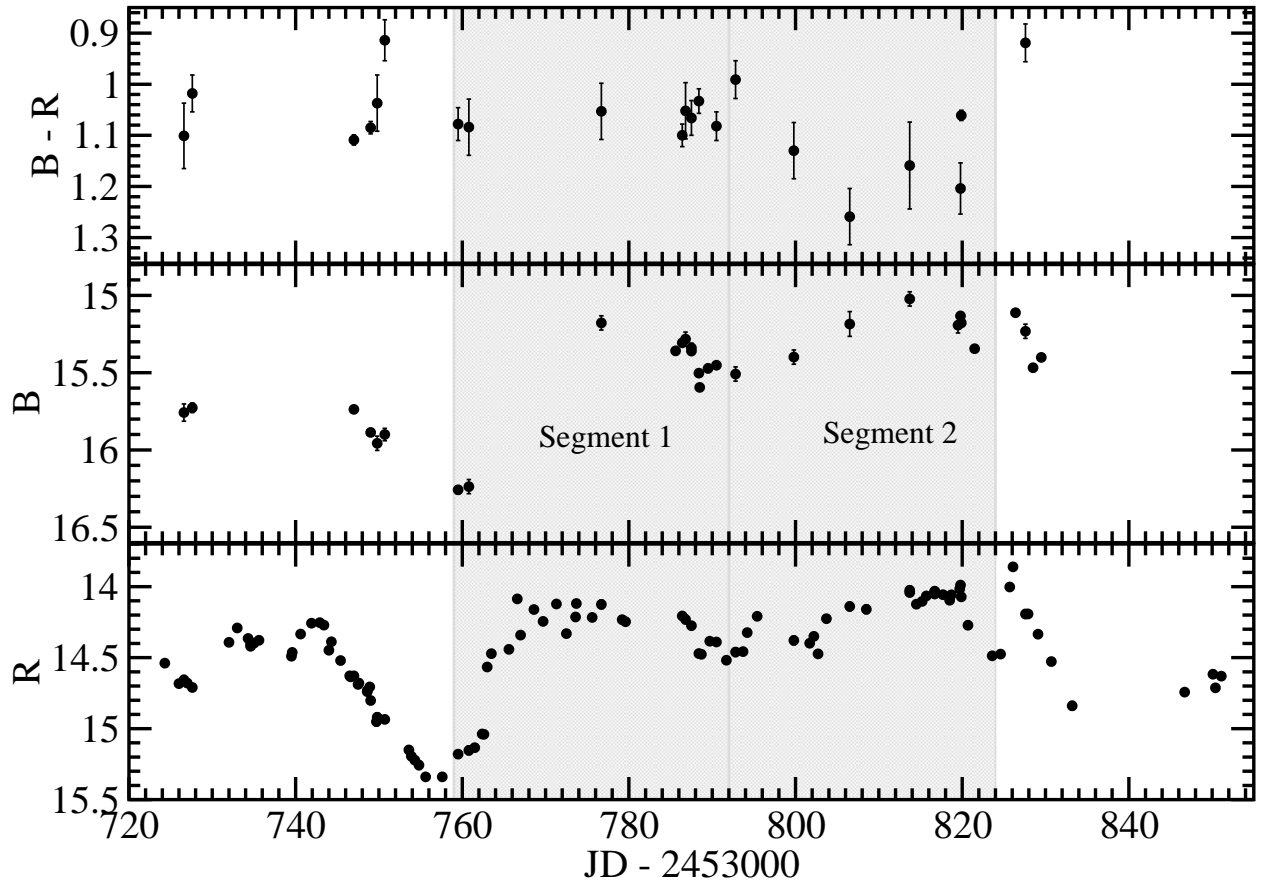


Fig. 2.— Light curve of the B and R magnitudes and the B - R color index of 3C 279 over the duration of the entire campaign.

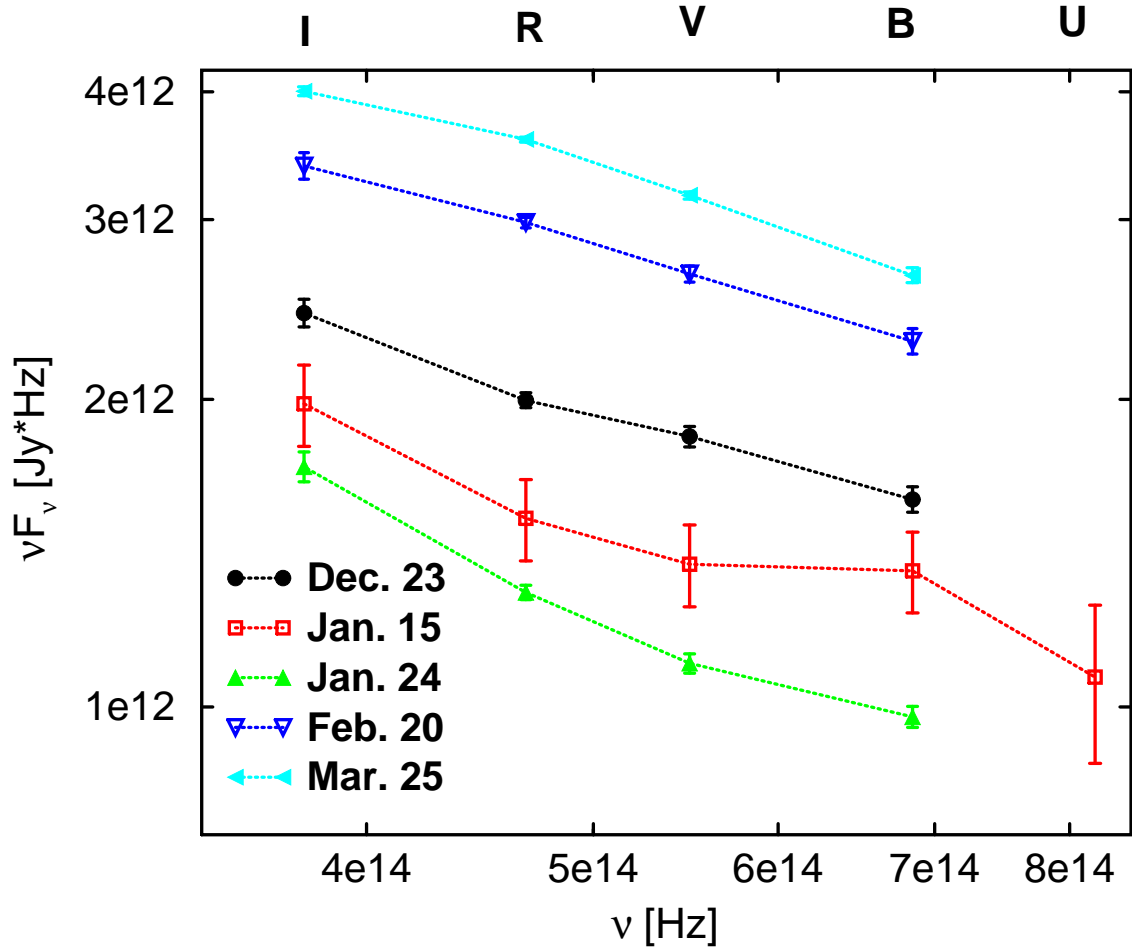


Fig. 3.— Snapshot optical (BVRI) continuum spectra for 5 epochs during our campaign. All measurements for each individual spectrum were taken within ≤ 20 min. of each other.

quasar 3C 454.3 (Villata et al. 2006), where it could be interpreted as a “little blue bump” due to the unresolved contribution from optical emission lines in the $\sim 2000 - 4000 \text{ \AA}$ wavelength range in the rest frame of the quasar, in particular from Fe II and Mg II (Raiteri et al. 2007). In order to test whether such an interpretation would also be viable in the case of 3C 279, we have compiled several simultaneous snap-shot optical continuum (BVRI) spectra at various brightness levels (Fig. 3). All measurements for each individual spectrum displayed in Fig. 3 have been taken within ≤ 20 min. of each other. Only the spectrum of Jan. 15 shows a significant deviation from a pure power-law in the B band; and in that case, there was simultaneous U band coverage, which matched a straight power-law extrapolation of the VRIJHK spectrum. If the spectral upturn towards the blue end of the spectrum were due to an unresolved Mg II / Fe II line contribution, it should emerge even more clearly in the Jan. 24 spectrum, which is characterized by a lower optical continuum flux level than the Jan. 15 spectrum. Therefore, the compilation of spectra in Fig. 3 does not provide any support for the existence of an essentially non-variable continuum component at the blue end of the spectrum. For this reason, we believe that the color changes that we found in our data are in fact intrinsic to the blazar jet emission.

Fig. 4 illustrates our impression from Fig. 2, that there is no clear overall trend of source (R-band) brightness with optical spectral hardness. However, the figure clearly illustrates that the scatter of the B – R color index is significantly larger at larger source brightness, indicating that spectral variability is more likely to occur when the source is bright. Specifically, for $R > 14.5$, the data is consistent with a roughly constant value of B – R = 1.09, corresponding to a spectral index of $\alpha_o = 1.9$ for a power-law continuum spectrum with $F_{\nu,o}[\text{Jy}] \propto \nu^{-\alpha_o}$. At brightness levels $R < 14.5$, spectral variability by $\Delta(B - R) \lesssim 0.35$, corresponding to $\Delta\alpha_o \lesssim 0.85$, is observed.

In Fig. 5, we focus on two ~ 1 -month optical flares, around mid-Jan. – mid-Feb. 2006, and late Feb. – late March 2006, as indicated by the gray shaded segments 1 and 2, respectively, in Fig. 2. The number labels in the color-magnitude diagrams in Fig. 5 indicate the time ordering of the points. While there is no obvious trend discernible in Segment 1, Segment 2 suggests the presence of a spectral hysteresis pattern: The spectral softening around JD 2453790 – 2453806 (Feb. 23 – Mar. 11), already mentioned above, precedes the main brightness increase. Subsequently, the optical continuum hardens while the source is still in a bright state. We need to caution that due to the poor sampling of the B band light curve during segment 2, the significance of the tentative hysteresis found here may be questionable. However, such hysteresis would naturally lead to a B-band time lag behind the R-band, for which we do find a 3.9σ evidence from a discrete correlation function analysis as described in the following section.

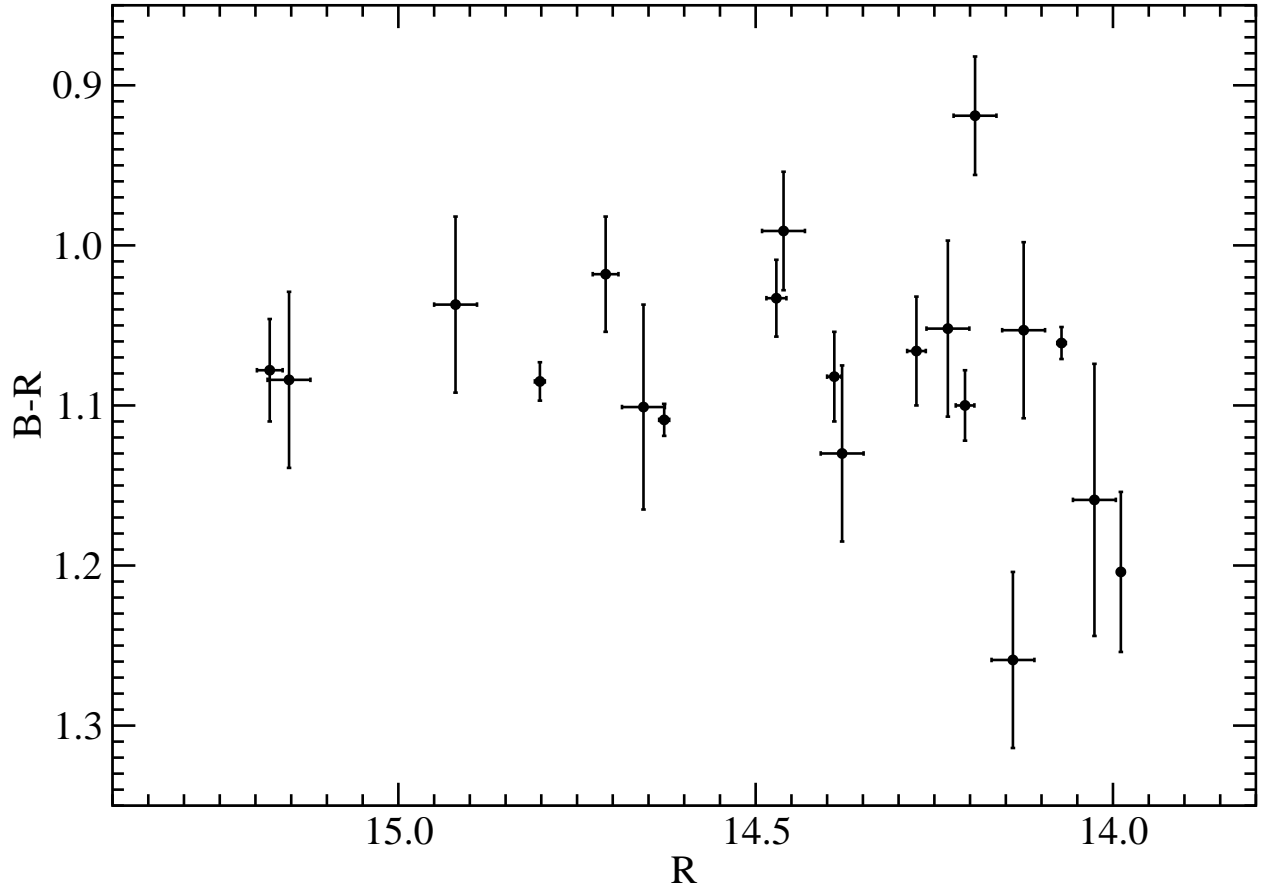


Fig. 4.— Color-magnitude diagram for the entire campaign period.

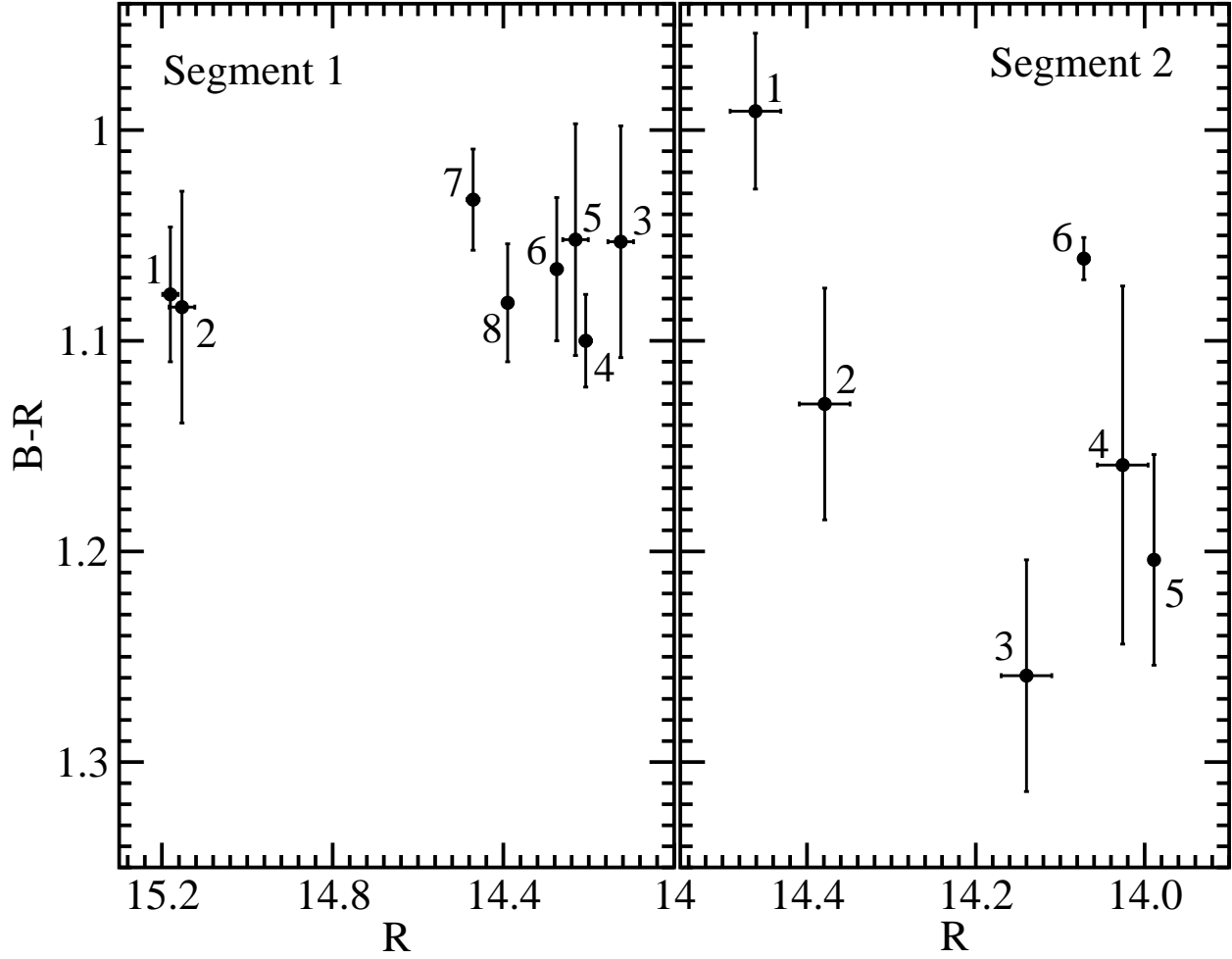


Fig. 5.— Color-magnitude diagrams for the two time segments marked in Fig. 2, with time ordering indicated by the numbers in the two panels.

To our knowledge, such a spectral hysteresis has never been observed at optical wavelengths for any flat-spectrum radio quasar. It is reminiscent of the spectral hysteresis occasionally seen at X-ray energies in high-frequency peaked BL Lac objects (HBLs, e.g. Takahashi et al. 1996; Fossati et al. 2000; Kataoka et al. 2000). However, the spectral hysteresis observed in the X-rays of HBLs is generally clockwise (i.e., spectral hardening precedes flux rise; softening precedes flux decline), and can be interpreted as the synchrotron signature of fast acceleration of ultrarelativistic electrons, followed by a gradual decline on the radiative cooling time scale (e.g., Kataoka et al. 2000; Kusunose, Takahara, & Li 2000; Li & Kusunose 2000; Böttcher & Chiang 2002). In our case, the direction of the spectral hysteresis is counterclockwise (i.e., spectral softening precedes the flux rise; spectral hardening precedes flux decline). Possible physical implications of such hysteresis phenomena will be discussed in §6.

4. Inter-band cross-correlations and time lags

The result of an occasional counterclockwise hysteresis in 3C 279, as found in the previous section, immediately suggests the existence of a characteristic time lag of higher-frequency behind lower-frequency variability. In order to investigate this, we evaluated the discrete correlation function (DCF, Edelson & Krolik 1988) between the R band and the other optical light curves. In our notation, a positive value of the time lag $\Delta\tau$ would indicate a lag of the R-band light curve behind the comparison light curve. As mentioned earlier, the radio (and near-IR) light curves are too sparsely sampled and yielded no significant features in the DCF. Fig. 6 shows the DCF between the R band and the V band (top panel) and the B band (bottom panel), using a sampling time scale of $\Delta\tau = 1$ d. We have done the same analysis using various other values of $\Delta\tau$, which yielded results consistent with the ones described below. We chose to show the results for $\Delta\tau = 1$ d because they provided the best compromise between dense time scale sampling and reduction of error bars.

The DCFs reveal clear correlations between the different optical wavebands, with peak values around 1. This confirms our previous impression from inspection by eye, that the variability patterns in all optical wavebands track each other very closely.

The resulting DCFs have then been fitted with a symmetric Gaussian, $F_0 e^{-(\tau-\tau_0)^2/(2\sigma^2)}$. This analysis yields non-zero offsets of the best-fit maxima, τ_0 at the $\sim 3 - 4\sigma$ level. Specifically, we find $\tau_0 = (-1.14 \pm 0.48)$ d for the V band and $\tau_0 = (-3.75 \pm 0.96)$ d for the B band. This indicates a hard time lag of higher-frequency variability behind the variability at lower frequencies in the B-V-R frequency range. However, this trend does not continue into the I band. This is illustrated in Fig. 7, where we plot the best-fit time lags as a function of

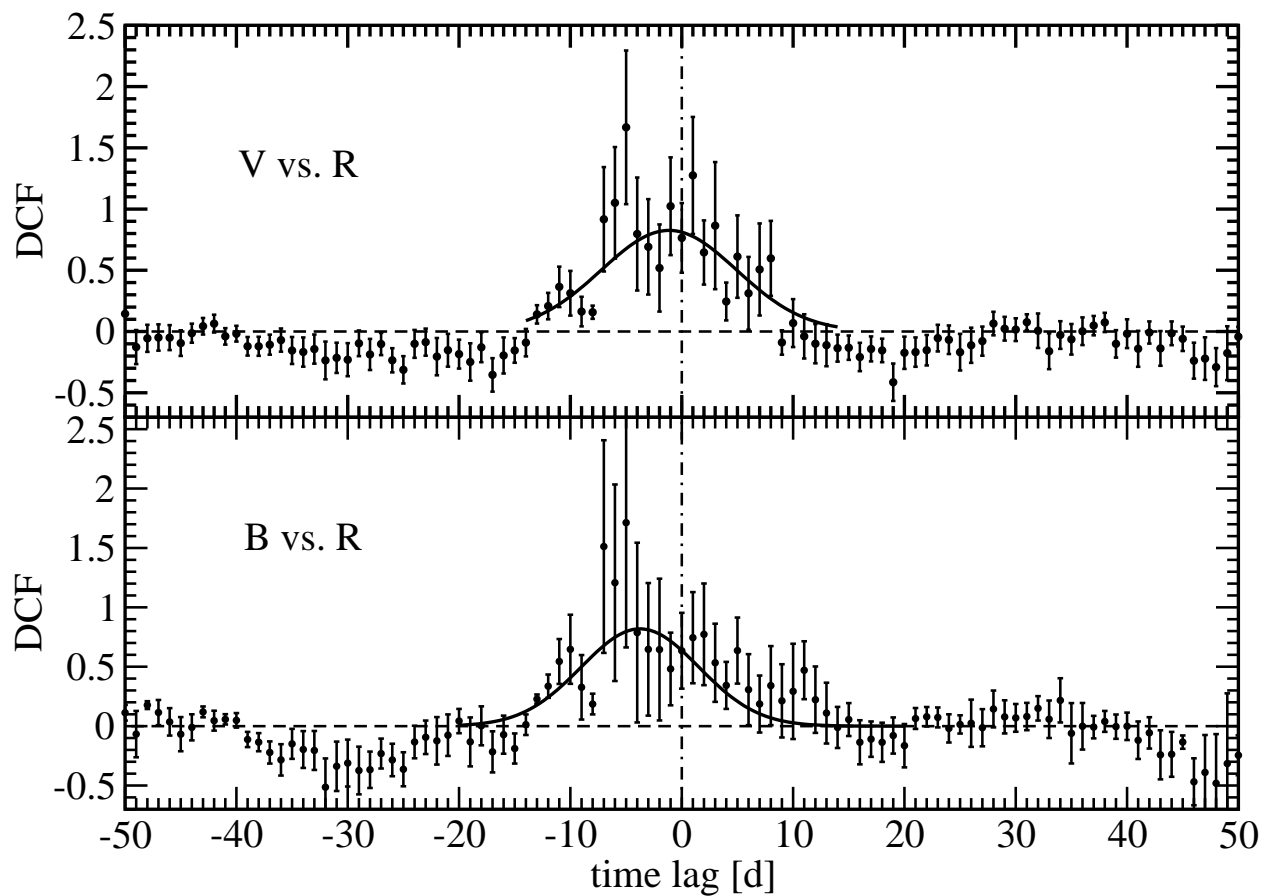


Fig. 6.— Discrete correlation functions between V and R (top panel), and B and R (bottom panel), respectively. The solid curves indicate the best fit with a symmetric Gaussian. This leads to a best-fit maximum correlation at $\tau_0 = (-1.14 \pm 0.48)$ d for the V band and $\tau_0 = (-3.75 \pm 0.96)$ d for the B band, indicating a lag of the V and B band light curves behind the R-band.

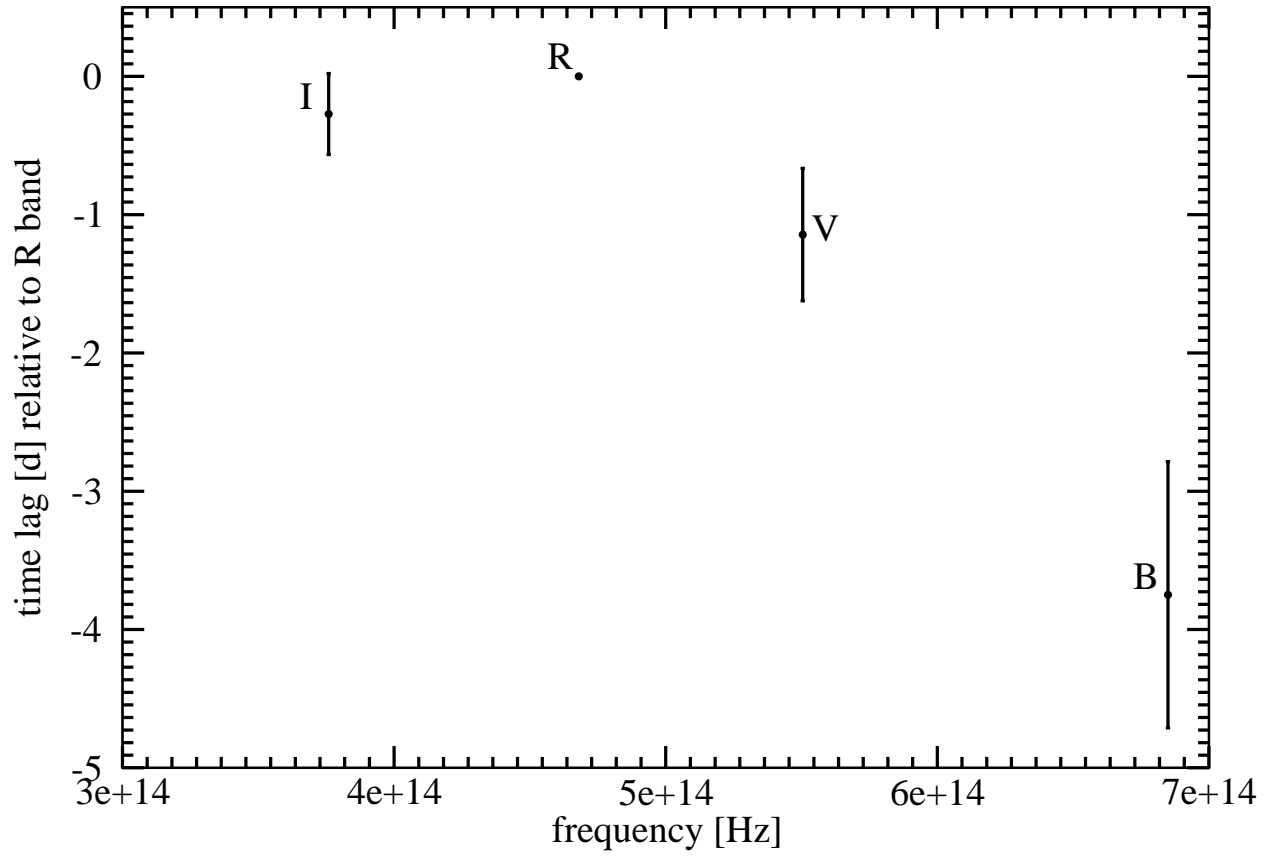


Fig. 7.— Best-fit time lag of the R band vs. B, V, R, and I bands, as a function of frequency.

photon frequency. However, we need to add a note of caution: The rather sparse sampling of the B- and V-band light curves leads to large error bars on the DCFs. Clearly, alternative, more complex representations, e.g., multiple Gaussians and/or asymmetric functions, will also provide acceptable fits to the observed DCFs and may lead to different quantitative results concerning the involved time lags. Future observations with denser B- and V-band sampling are needed in order to test the robustness of the trend found here.

The hard lag found in this analysis may be physically related to the $\sim 2 - 3$ d time lag of the soft X-ray spectral index behind the flux in *ROSAT* observations of 3C 279 in December 1992 – January 1993 (Pian et al. 1999). Possible physical interpretations will be discussed in §6.

5. Broad-band spectral energy distribution

The most complete broadband coverage of 3C 279 during our campaign was obtained on January 15, 2006. On that day, the only near-infrared (JHK) exposures were taken with the NOT, and simultaneous radio observations at 5, 8, 22, and 37 GHz were available as well. This is also within the time window of the X-ray and soft γ -ray observations, although in most cases, a meaningful extraction of spectral information required the integration over most of the high-energy observing period, January 13 – 20, 2006 (Collmar et al. 2007a). The total snap-shot SED composed of all available radio, near-IR, optical, X-ray, and soft γ -ray observations around January 15, 2006 is displayed in Fig. 8, where all near-IR and optical data are taken within $\pm 1/2$ hr of UT 05:00 on January 15. The figure compares the January 2006 SED to previous SEDs from the bright flare during the first *EGRET* observing epoch in June 1991, the low state of December 1992 / January 1993 (both SEDs adapted from Hartman et al. 2001a), and a previous multiwavelength campaign around *INTEGRAL* AO-1 observations of 3C 279 in a low state in June 2003 (Collmar et al. 2004).

While the optical (presumably synchrotron) emission component clearly indicates that the source was in an elevated state compared to previous low states, the simultaneous X-ray – soft- γ -ray spectrum is perfectly consistent with the low-state spectra of 1992/1993 and 2003. This is a very remarkable result and will be discussed in detail in a companion paper about the results of the entire multiwavelength campaign (Collmar et al. 2007b).

The NIR – optical continuum can be very well represented by a single power-law with a spectral index of $\alpha_o = 1.64 \pm 0.04$, corresponding to an underlying non-thermal electron distribution with a spectral index of $p = 4.28 \pm 0.08$, if the optical continuum is synchrotron emission. As already pointed out in Hartman et al. (2001a) for a comparison between various

3C279

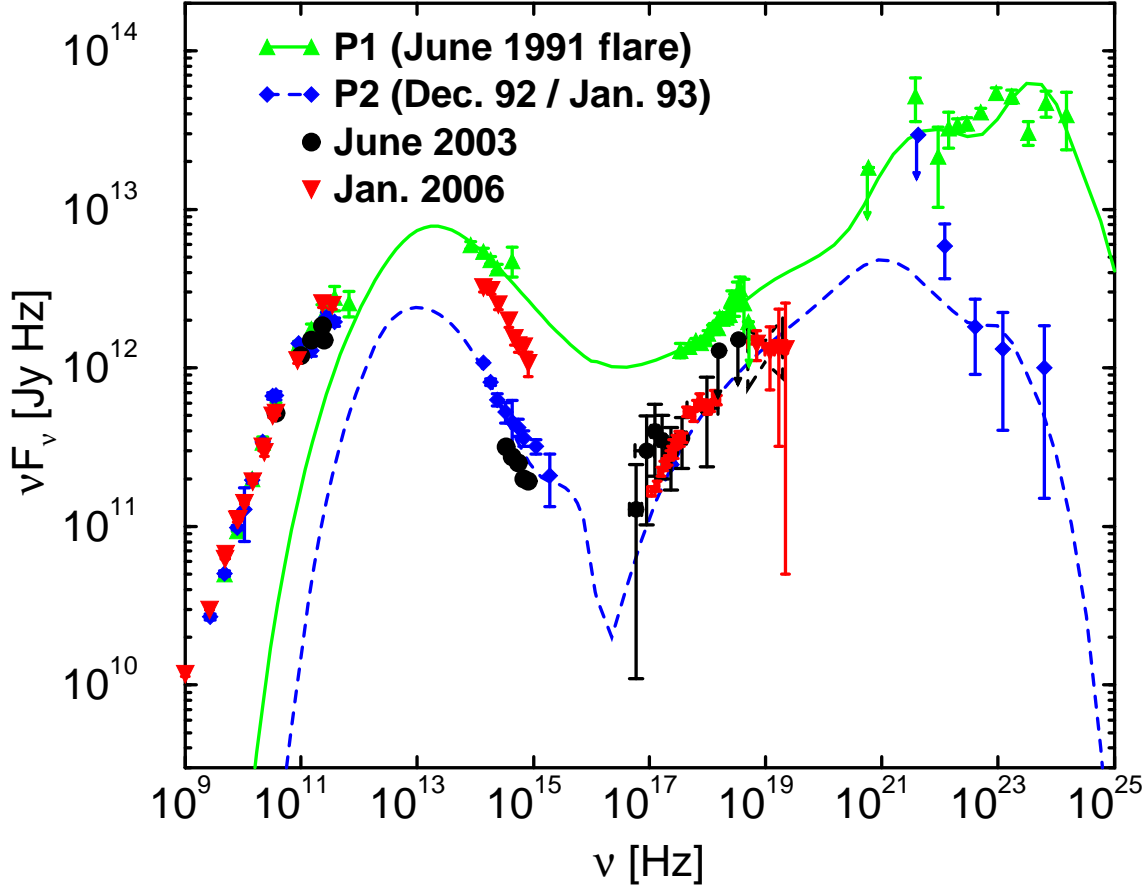


Fig. 8.— Simultaneous snap-shot spectral energy distributions of 3C 279 at various epochs. Data pertaining to the multiwavelength campaign in January 2006 are plotted with red triangles. All IR and optical data were taken within $\pm 1/2$ hr of UT 05:00 on Jan. 15, 2006; the X-ray and soft γ -ray data represent the time-averaged spectra throughout the respective observing windows in Jan. 2006, which included Jan. 15 for all instruments. Model fits to the *EGRET* P1 and P2 SEDs are calculated using a time-dependent leptonic (SSC + EC) jet model, and taken from Hartman et al. (2001a). The June 2003 SED is from Collmar et al. (2004).

EGRET observing epochs over ~ 10 years and confirmed by our campaign data on time scales of weeks – months (see §3), the optical spectral index in 3C 279 does not show any systematic correlation with the brightness state of the source, and Fig. 8 indicates that in our high-state observations of 2006, the continuum spectral slope is not significantly different from the slopes observed in the low states of 1992/1993 and 2003.

6. Discussion

In this section, we discuss some general physical implications and constraints that our results can place on source parameters. In the following discussion, we will parameterize the magnetic field in units of Gauss, i.e., $B = 1 B_G$ Gauss, and the Doppler boosting factor $D = (\Gamma[1 - \beta_\Gamma \cos \theta_{\text{obs}}])^{-1}$ in units of 10, i.e., $D = 10 D_1$ where Γ is the bulk Lorentz factor of the emitting region, $\beta_\Gamma c$ is the corresponding speed, and θ_{obs} is the observing angle. The characteristic variability time scale is of the order of 1 – a few days, so we write $t_{\text{var}}^{\text{obs}} \equiv 1 t_{\text{var,d}}^{\text{obs}}$. In the same sense, we parameterize the time lag of the B band behind the R band as $\tau_{\text{BR}}^{\text{obs}} \equiv 1 \tau_{\text{BR,d}}^{\text{obs}}$ d with $\tau_{\text{BR,d}}^{\text{obs}} \sim 3$. The observed variability time scale yields an estimate of the size of the emitting region, $R \equiv 10^{15} R_{15}$ cm through $R \lesssim c D / (1 + z) t_{\text{var}}^{\text{obs}}$. We find $R_{15} \lesssim 17 D_1 t_{\text{var,d}}^{\text{obs}}$.

The (co-moving) energies of electrons emitting synchrotron radiation at their characteristic peak frequencies in the R and B bands are

$$\begin{aligned} \gamma_R &= 3.7 \times 10^3 (B_G D_1)^{-1/2} \\ \gamma_B &= 4.5 \times 10^3 (B_G D_1)^{-1/2} \end{aligned} \quad (1)$$

The steep underlying electron spectrum with $p = 4.5$, inferred from the steep optical continuum, might indicate that the entire optical spectrum is produced by electrons in the fast-cooling regime. This implies that the radiative cooling time scale of electrons emitting synchrotron radiation in the optical regime is shorter than the characteristic escape time scale of those electrons. The respective time scales in the co-moving frame, t'_{esc} and t'_{cool} can be written as

$$\begin{aligned} t'_{\text{esc}} &\equiv \eta \frac{R}{c} \lesssim 5.7 \times 10^5 \eta D_1 t_{\text{var,d}}^{\text{obs}} \text{ s} \\ t'_{\text{cool}} &= \frac{\gamma}{\dot{\gamma}_{\text{rad}}} \sim 7.7 \times 10^7 B_G^{-1} \gamma^{-1} (1 + k)^{-1} \text{ s} \end{aligned} \quad (2)$$

where $\eta \geq 1$ is the escape time scale parameter (as defined in the first line of eq. 2), and k is a correction factor accounting for radiative cooling via Compton losses in the Thomson

regime in a radiation field with an energy density $u'_{\text{rad}} \equiv k u'_{\text{sy}}$. Requiring that the cooling time scale is shorter than the escape time scale, at least for electrons emitting in the R band, leads to a lower limit on the magnetic field:

$$B \gtrsim B_c \equiv 1.3 \times 10^{-3} (1+k)^{-2} \eta^{-1} (t_{\text{var,d}}^{\text{obs}})^{-2} \text{ G} \quad (3)$$

which does not seem to pose a severe constraint, given the values of $B \sim$ a few G typically found for other FSRQs and also for 3C 279 from previous SED modeling analyses (e.g., Hartman et al. 2001a).

Another estimate of the co-moving magnetic field can be found by assuming that the dominant portion of the time-averaged synchrotron spectrum is emitted by a power-law spectrum of electrons with $N_e(\gamma) = n_0 V_B \gamma^{-p}$ for $\gamma_1 \leq \gamma \leq \gamma_2$; here, V_B is the co-moving blob volume, and we use $p = 4.5$ as a representative value inferred from the optical continuum slope. The normalization constant $n_0 = n_e (1-p) / (\gamma_2^{1-p} - \gamma_1^{1-p})$ is related to the magnetic field through an equipartition parameter $e_B \equiv u'_B / u'_e$ (in the co-moving frame). Note that this equipartition parameter only refers to the energy density of the electrons, not accounting for a (possibly dominant) energy content of a hadronic matter component in the jet. Under these assumptions, the magnetic field can be estimated as described, e.g., in Böttcher et al. (2003). Taking the νF_ν peak synchrotron flux f_ϵ^{sy} at the dimensionless synchrotron peak photon energy $\epsilon_{\text{sy}} \equiv E_{\text{pk,sy}} / (m_e c^2) \approx 3 \times 10^{-7}$ as $\sim 10^{-10}$ ergs $\text{cm}^{-2} \text{ s}^{-1}$, we find

$$B \gtrsim B_{\text{eB}} \equiv 1.86 D_1^{-13/7} e_B^{2/7} (t_{\text{var,d}}^{\text{obs}})^{-1} \text{ G}. \quad (4)$$

This constitutes a more useful and realistic magnetic-field estimate than eq. 3. If, indeed, the optical emission is synchrotron emission from a fast-cooling electron distribution, then electrons have been primarily accelerated to a power-law distribution with an injection index of $q = p - 1 = 3.5$. This is much steeper than the canonical spectral index of $q \sim 2.2 - 2.3$ found for acceleration on relativistic, parallel shocks (e.g., Gallant, Achterberg & Kirk 1999; Achterberg et al. 2001), and could indicate an oblique magnetic-field orientation (e.g., Ostrowski & Bednarz 2002; Niemiec & Ostrowski 2004), which would yield a consistent picture with the predominantly perpendicular magnetic-field orientation observed on parsec-scales (Jorstad et al. 2004; Ojha et al. 2004; Lister & Homan 2005). The observed hard lag (B vs. R) may then be the consequence of a gradual spectral hardening of the electron acceleration (injection) spectrum throughout the propagation of a relativistic shock front along the jet. Such a gradual hardening of the electron acceleration spectrum could be the consequence of the gradual build-up of hydromagnetic turbulence through the relativistic two-stream instability (see, e.g., Schlickeiser et al. 2002). This turbulence would harden the rel-

ativistic electron distribution via 2nd-order Fermi acceleration processes (Virtanen & Vainio 2005). Such a scenario would imply a length scale for the build-up of turbulence of $\Delta r \sim c \tau_{\text{BR}}^{\text{obs}} D \Gamma / (1 + z) \sim 5.6 \times 10^{-2} \tau_{\text{BR,d}}^{\text{obs}} D_1 \Gamma_1 \sim 0.2$ pc for the characteristic values of 3C 279.

Alternatively, the acceleration process could become more efficient along the jet if the magnetic-field configuration gradually evolves into a more quasi-parallel one, on the same length scale of ~ 0.2 pc as estimated above. However, this scenario might be in conflict with the predominantly perpendicular magnetic-field orientation seen in the jets of 3C 279 on pc scales.

The hard lag in the optical regime may also be indicative of a slow acceleration mechanism, with an acceleration time scale of the order of the observed B vs. R lag. This would imply an acceleration rate of

$$\dot{\gamma}_A \sim \frac{\gamma_B - \gamma_R}{\tau_{\text{BR}}} \sim 6.8 \times 10^{-2} (\tau_{\text{BR,d}}^{\text{obs}})^{-1} \left(\frac{D_1}{B_G} \right)^{1/2} \text{ s}^{-1}. \quad (5)$$

In this scenario, electrons could only be accelerated to at least γ_B , if the acceleration rate of eq. 5 is larger than the absolute value of the radiative (synchrotron + Compton) cooling rate corresponding to eq. 2. This imposes an upper limit on the magnetic field:

$$B \lesssim B_{\text{acc}} \sim 0.42 D_1^{1/3} (\tau_{\text{BR,d}}^{\text{obs}})^{-2/3} (1 + k)^{-2/3} \text{ G}. \quad (6)$$

This can be combined with the estimate in eq. 4 to infer a limit on the magnetic-field equipartition parameter:

$$e_B \lesssim e_{B,\text{acc}} \sim 5.8 \times 10^{-3} D_1^{23/3} (\tau_{\text{BR,d}}^{\text{obs}})^{-7/3} (t_{\text{var,d}}^{\text{obs}})^{7/2} (1 + k)^{-7/3}. \quad (7)$$

Based on this equipartition parameter, one can use the magnetic-field estimate of eq. 4 to estimate the total amount of co-moving energy contained in the emission region at any given time:

$$E'_e \sim \frac{4}{3} \pi R^3 \frac{u'_B}{e_B} \sim 2.5 \times 10^{49} D_1^{-4} \tau_{\text{BR,d}}^{\text{obs}} (t_{\text{var,d}}^{\text{obs}})^{-1/2} (1 + k) \text{ erg} \quad (8)$$

Assuming that the bulk of this energy is dissipated within the characteristic variability time scale, one can estimate the power in relativistic electrons in the jet:

$$L_{\text{jet}} \sim \frac{E'_e}{t'_{\text{var}}} \sim 4.5 \times 10^{43} D_1^{-5} \tau_{\text{BR,d}}^{\text{obs}} (t_{\text{var,d}}^{\text{obs}})^{-3/2} (1 + k) \text{ ergs s}^{-1}. \quad (9)$$

Previous modeling works of the SEDs of FSRQs in general and 3C 279 in particular indicated characteristic magnetic field values of a few Gauss, in approximate equipartition with the ultrarelativistic electron population. The unusually low equipartition parameter in eq. 7 could therefore pose a problem for the slow-acceleration scenario. Note, however, the very strong dependence of e_B on the Doppler factor ($\propto D^{23/3}$). A Doppler factor $D \sim 20$ could account for equipartition parameters of the order of one. Also, the energy requirements of eqs. 8 and 9 seem reasonable, and there does not appear to be a strict argument that would rule this scenario out.

Another scenario one could think of would be based on a decreasing magnetic field along the blazar jet, leading to a gradually increasing cooling break in the underlying electron distribution. This would require that the cooling time scale for electrons emitting synchrotron radiation in the optical regime would be equal to or longer than the escape time scale. Thus, the inequality in eq. 3 would be reversed. This would require unreasonably low magnetic fields. Furthermore, this scenario would be in conflict with the typically observed unbroken snap-shot power-law continuum spectra throughout the optical-IR range. Therefore, this idea may be ruled out.

7. Summary

We have presented the results of an optical-IR-radio monitoring campaign on the prominent blazar-type flat-spectrum radio quasar 3C 279 by the WEBT collaboration in January – April 2006, around Target of Opportunity X-ray and soft γ -ray observations with *Chandra* and *INTEGRAL* in mid-January 2006. Previously unpublished radio and optical data from several weeks leading up to the ToO trigger are also included.

The source exhibited substantial variability of flux and spectral shape, in particular in the optical regime, with a characteristic time scale of a few days. The variability patterns throughout the optical BVRI bands were very closely correlated with each other, while there was no significant evidence for a correlation between the optical and radio variability. After the trigger flux level for the *Chandra* and *INTEGRAL* ToOs was reached on Jan. 5, 2006, the optical flux decayed smoothly by 1.1 mags. within 13 days, until the end of the time frame of the X-ray and γ -ray observations. The decay could be well described by an exponential decay with a decay time scale of $\tau_d = 12.8$ d. The flux then recovered to approximately the pre-dip values in a much more erratic way, including a $\sim 0.5^{\text{mag}}$ rise within ~ 1 d.

A discrete correlation function analysis between different optical (BVRI) bands indicates a hard lag with a time delay increasing with increasing frequency, reaching ~ 3 d for the lag

of B behind R. This appears to be accompanied by a single indication of counterclockwise spectral hysteresis in a color-intensity diagram (B-R vs. R). Thus, spectral hardening during flares appears delayed with respect to a rising optical flux. There is no consistent overall trend of optical spectral hardness with source brightness. However, our data indicate that the source displays a rather uniform spectral slope of $\alpha_o \sim 1.9$ at moderate flux levels ($R > 14.5$), while spectral variability seems common at high flux levels ($R < 14.5$).

The occasional optical spectral hysteresis, in combination with the very steep IR-optical continuum spectral index of $\alpha_o \sim 1.5 - 2.0$, may indicate a highly oblique magnetic field configuration near the base of the jet, leading to inefficient particle acceleration and a very steep electron injection spectrum. As the emission region propagates along the jet, a gradual hardening of the primarily injected ultrarelativistic electron distribution may be caused by the gradual build-up of hydromagnetic turbulence, which could lead to a gradually increasing contribution of second-order Fermi acceleration. This would imply a length scale of the build-up of hydromagnetic turbulence of $\Delta r \sim 0.2$ pc.

An alternative explanation of the hard lag may be a slow acceleration mechanism by which relativistic electrons are accelerated on a time scale of several days. However, even though this model can plausibly explain the observed variability trends and overall luminosity of the source, it requires an unusually low magnetic field in the emitting region of $B \lesssim 0.2$ G, unless rather high Doppler factors of $D \gtrsim 20$ are assumed. Such a small magnetic field would be about an order of magnitude lower than inferred from previous analyses of simultaneous SEDs of 3C 279 and other flat-spectrum radio quasars with similar properties.

The work of M. Böttcher and S. Basu was partially supported by NASA through INTEGRAL GO grant award NNG 06GD57G and the Chandra GO program (administered by the Smithsonian Astrophysical Observatory) through award no. GO6-7101A. The Metsähovi team acknowledges the support from the Academy of Finland. YYK is a research fellow of the Alexander von Humboldt Foundation. RATAN-600 observations were partly supported by the Russian Foundation for Basic Research (project 05-02-17377). The St. Petersburg team was supported by the Russian Foundation for Basic Research through grant 05-02-17562.

REFERENCES

- Achterberg, A., Gallant, Y. A., Kirk, J. G., & Guthmann, A. W., 2001, MNRAS, 328, 393
Bach, U., et al., 2007, A&A, 464, 175
Bednarek, W., 1998, A&A, 336, 123

- Böttcher, M., 2007a, in proc. “The Multimessenger Approach to Gamma-Ray Sources”, ApSS, in press (astro-ph/0608713)
- Böttcher, M., 2007b, in proc. “The Central Engine of Active Galactic Nuclei”, ASPCS, in press
- Böttcher, M., & Bloom, S. D., 2000, AJ, 119, 469
- Böttcher, M., & Chiang, J., 2002, ApJ, 581, 127
- Böttcher, M., Mause, H., & Schlickeiser, R., 1997, A&A, 324, 395
- Böttcher, M., et al., 2003, ApJ, 596, 847
- Böttcher, M., et al., 2005, ApJ, 631, 169
- Collmar, W., et al., 2004, in proc. of 5th INTEGRAL Workshop, ESA-SP 552, Ed.: B. Battrick, p. 555
- Collmar, W., et al., 2007a, in proc. of 6th INTEGRAL Workshop, ESA-SP, in press
- Collmar, W., et al., 2007b, in preparation
- Cotton, W. D., et al., 1979, ApJ, 229, L115
- Edelson, R. A., & Krolik, J. H., 1988, ApJ, 333, 646
- Floyd, D. J. E., Kukula, M. J., Dunlop, J. S., McLure, R. J., Miller, L., Percival, W. J., Baum, S. A., & O’Dea, C. P., 2004, MNRAS, 355, 196
- Fossati, G., et al., 2000, ApJ, 541, 166
- Gallant, Y. A., Achterberg, A., & Kirk, J. G., 1999, A&AS, 138, 549
- González-Pérez, J. N., Kidger, M. R., & Martín-Luis, F., 2001, AJ, 122, 2055
- Hartman, R. C., et al., 1996, ApJ, 461, 698
- Hartman, R. C., et al., 1999, ApJS, 123, 79
- Hartman, R. C., et al., 2001a, ApJ, 553, 683
- Hartman, R. C., et al., 2001b, ApJ, 558, 583
- Helmboldt, J. F., et al., 2007, ApJ, 658, 203

- Homan, D. C., Lister, M. L., Kellermann, K. I., Cohen, M. H., Ros, E., Zensus, J. A., Kadler, M., & Vermeulen, R. C., 2003, *ApJ*, 589, L9
- Jorstad, S. G., Marscher, A. P., Lister, M. L., Stirling, A. M., Cawthorne, T. V., Gómez, J.-L., & Gear, W. K., 2004, *AJ*, 127, 3115
- Kartaltepe, J. S., & Balonek, T. J., 2007, *ApJ*, 133, 2866
- Kataoka, J., Takahashi, T., Makino, F., Inoue, S., Madejski, G. M., Tashiro, M., Urry, C. M., & Kubo, H., 2000, *ApJ*, 528, 243
- Kirk, J. G., Rieger, F. M., & Mastichiadis, A., 1998, *A&A*, 333, 452
- Kusunose, M., Takahara, F., & Li, H., 2000, *ApJ*, 536, 299
- Li, H., & Kusunose, M., 2000, *ApJ*, 536, 729
- Lister, M. L., & Homan, D. C., 2005, *AJ*, 130, 1389
- Maraschi, L., et al., 1994, *ApJ*, 435, L91
- Mattox, J. R., Hartman, R. C., & Reimer, O., 2001, *ApJS*, 135, 155
- Moderski, R., Sikora, M., Blazejowski, M., 2003, *A&A*, 406, 855
- Mücke, A., & Protheroe, R. J., 2001, *Astropart. Phys.*, 15, 121
- Mücke, A., Protheroe, R. J., Engel, R., Rachen, J. P., & Stanev, T., 2003, *Astropart. Phys.*, 18, 593
- Nandikotkur, G., Jahoda, K. M., Hartman, R. C., Mukherjee, R., Sreekumar, P., Böttcher, M., Sambruna, R. M., & Swank, J. H., 2007, *ApJ*, 657, 705
- Niemiec, J., & Ostrowski, M., 2004, *ApJ*, 610, 851
- Ojha, R., Homan, D. C., Roberts, D. H., Wardle, J. F. C., Aller, M. F., Aller, H. D., & Hughes, P. A., 2004, *ApJS*, 150, 187
- Ostrowski, M., & Bednarz, J., 2002, *A&A*, 394, 1141
- Pian, E., et al., 1999, *ApJ*, 521, 112
- Raiteri, C. M., Villata, M., Lanteri, L., Cavallone, M., & Sobrito, G., 1998, *A&AS*, 130, 495
- Raiteri, C. M., et al., 2001, *A&A*, 377, 396

- Raiteri, C. M., et al., 2005, *A&A*, 438, 39
- Raiteri, C. M., et al., 2006, *A&A*, 459, 731
- Raiteri, C. M., et al., 2007, *A&*, submitted
- Schlegel, D. J., Finkbeiner, D. P., & Davis, M., 1998, *ApJ*, 500, 525
- Schlickeiser, R., Vainio, R., Böttcher, M., Schuster, C., Lerche, I., & Pohl, M., 2002, *A&A*, 393, 69
- Sikora, M., Blazejowski, M., Begelman, M. C., & Moderski, R., 2001, *ApJ*, 554, 1; Erratum: *ApJ*, 561, 1154 (2001)
- Smith, P. S., & Balonek, T. J., 1998, *PASP*, 110, 1164
- Takahashi, T., et al., 1996, *ApJ*, 470, L89
- Teräsraanta, H., et al., 1998, *A&AS*, 132, 305
- Unwin, S. C., Biretta, J. A., Hodges, M. W., & Zensus, J. A., 1989, *ApJ*, 340, 117
- Villata, M., et al., 2000, *A&A*, 363, 108
- Villata, M., et al., 2002, *A&A*, 390, 407
- Villata, M., et al., 2004a, *A&A*, 421, 103
- Villata, M., et al., 2004b, *A&A*, 424, 497
- Villata, M., et al., 2006, *A&A*, 453, 817
- Villata, M., et al., 2007, *A&A*, 464, L5
- Virtanen, J. J. P., & Vainio, R., 2005, *ApJ*, 621, 313
- Wehrle, A. E., et al., 1998, *ApJ*, 497, 178
- Whitney, A. R., et al., 1971, *Science*, 173, 225
- Zakamska, N. L., et al., 2006, *ApJ*, 132, 1496